Supporting Information

Multiple chirality inversion of pyridine Schiff-base cholesterol-based metal-organic supramolecular polymers

Yanbin Wang[a], Chongtao Liu[a,b], Kuo Fu[b], Junxi Liang[a], Shaofeng Pang[a, *], Guofeng Liu[b, *]

[a] Chemical Engineering Institute, Key Laboratory of Environment-Friendly Composite Materials of the State Ethnic Affairs Commission, Northwest Minzu University, Lanzhou, Gansu, 730030, P. R. China

[b] Shanghai Key Laboratory of Chemical Assessment and Sustainability, Advanced Research Institute, School of Chemical Science and Engineering, Tongji University, Shanghai, 200092, P. R. China.

E-mail: liuguofeng@tongji.edu.cn; pangshaofeng2006@163.com

1 Experimental section

Instruments and methods. NMR spectra were recorded on a Bruker Advance III 600 Instrument (600 MHz) at ambient temperature. Circular dichroism (CD) spectra were obtained using JASCO 810 CD spectrometer with the bandwidth of 1.0 nm, scanning speed of 200 nm/min, and data integration time of 1 s. CD spectra of gels were recorded in the UV-vis region (250-600 nm) using a 0.1 mm quartz Scanning electron microscopy (SEM) was performed on a JEOL JSM-7600F microscope with an accelerating voltage of 5 kV. Before SEM measurements, samples were prepared by depositing dilute solutions of gels on silicon wafers, followed by drying and coating them with a thin layer of Pt to increase the contrast.

Material. Acetic anhydride, 3-aminophenol, 4-aldehyde pyridine, cholesteryl chloroformate, silver nitrate, manganese chloride, cobalt chloride, nickel chloride, copper chloride, zinc chloride, bismuth chloride, methanol, N ,N-dimethylformamide, potassium hydroxide, triethylamine (Et_3N)

Metallogel preparation. A typical procedure for the formation of metallogels in organic solvents is as follows: metal chloride was added into the solvents of mPMPCC with concentration of 16 mM. The metal chloride was dissolved completely upon ultrasound, and then the metallogels were obtained after several minutes of rest at room temperature.

Synthesis of mPMPCC. mPMAP was synthesized according to the previous report.[1] mPMAP (1.65 g, 8.33 mmol) in dry dichloromethane was added dropwise to a solution of cholesteryl chloroformate (3.75 g, 8.33 mmol) and triethylamine (0.50 mL, 3.61 mmol) in dichloromethane (50 mL) in an ice-water bath. After stirring at room temperature for 3 h, the solvent was evaporated under reduced pressure to obtain the off-white solid of crud product. The crud product was purified by methanol and petroleum ether to give mPMPCC (4.16 g, 6.82 mmol) in 82 % yield. ^{1}H NMR (400 MHz, $CDCl_3$, ppm): δ = 9.01 (s, 1H, Ar-H), 8.71 (d, 1H, Ar-H), 8.50 (s, 1H, N=CH), 8.28–8.30 (d, 1H, Ar-H), 7.40–7.44 (d, 1H, Ar-H), 7.24 (m, 4H, Ar-H), 5.42-5.44 (d, 1H, C=CH), 4.58–4.61 (m, 1H, O-CH), 2.47–2.51 (d, 2H, -CH_2), 2.00–2.04 (m, 2H, -CH_2), 1.95 (m, 1H, -CH), 1. 90 (m, 1H, -CH), 1.78–1.82 (m, 1H, -CH), 1.54 (m, 2H, -CH_2), 1.50–1.52 (m, 2H,-CH_2), 1.46–1.48 (m, 2H,-CH_2), 1.36–1.42 (m, 3H,-CH_3), 1.33 (s, 1H, -CH), 1.08–1.29 (m, 6H, -CH_2), 1.05 (s, 4H, -CH_2), 0.98-1.01 (m, 2H, -CH), 0.91-0.93 (d, 3H, -CH_3), 0.86-0.88 (s, 6H, -CH_3), 0.69 (s, 3H, -CH_3). ^{13}C NMR (100 MHz, $CDCl_3$, ppm): δ = 157.38, 153.00, 152.14, 151.01, 149.73, 149.08, 139.16, 134.94, 131.74, 123.84, 123.25, 121.88, 121.81, 79.02, 56.71, 56.16, 50.02, 45.81, 42.34, 39.74, 39.53, 37.97, 36.86, 36.84, 36.57, 36.20, 35.80, 31.93, 31.87, 28.23, 28.03, 27.67, 24.30, 23.84, 22.82, 22.57, 21.08, 19.30, 18.73, 11.88. EI-MS (m/z) for $C_{40}H_{54}N_2O_3$ calcd. 610.4134; found 611.4208 $[M+H]^+$.

2 Additional experimental data and figures

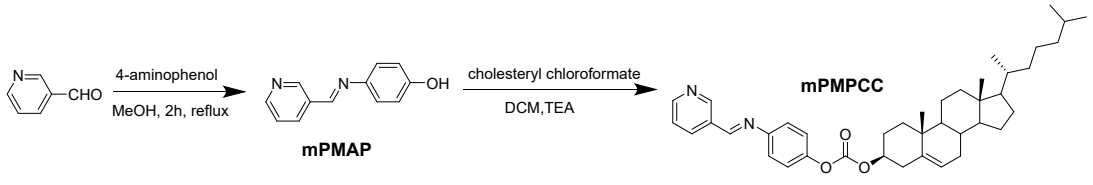

Scheme S1. Synthetic route of mPMPCC.

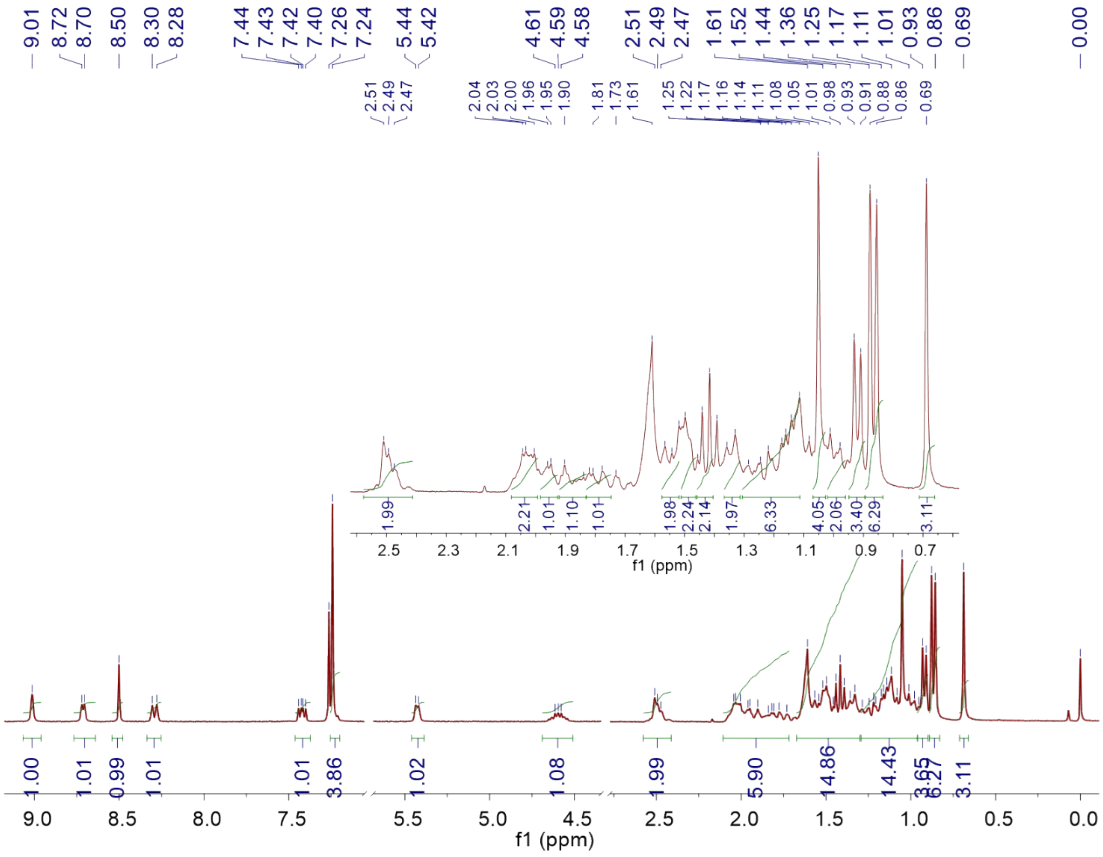

Figure S1. ^{1}H NMR spectrum of mPMPCC in $CDCl_3$.

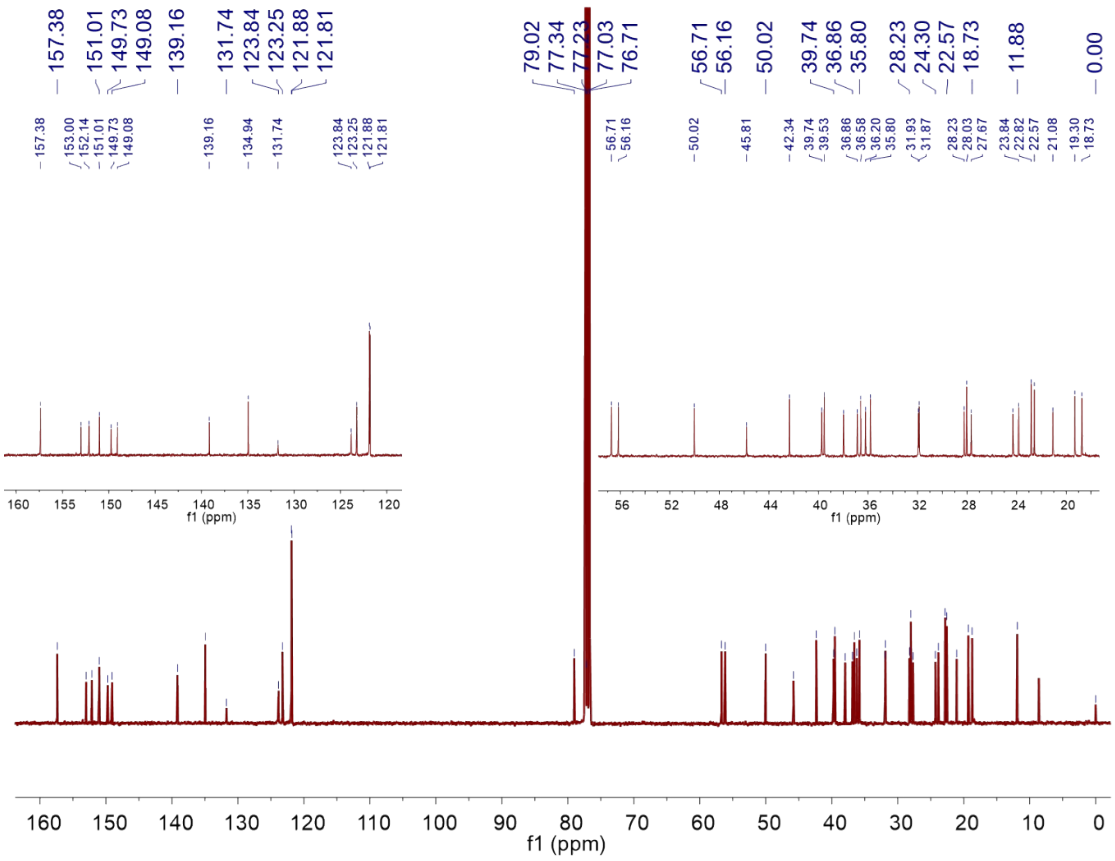

Figure S2. ^{13}C NMR spectrum of mPMPCC in $CDCl_3$.

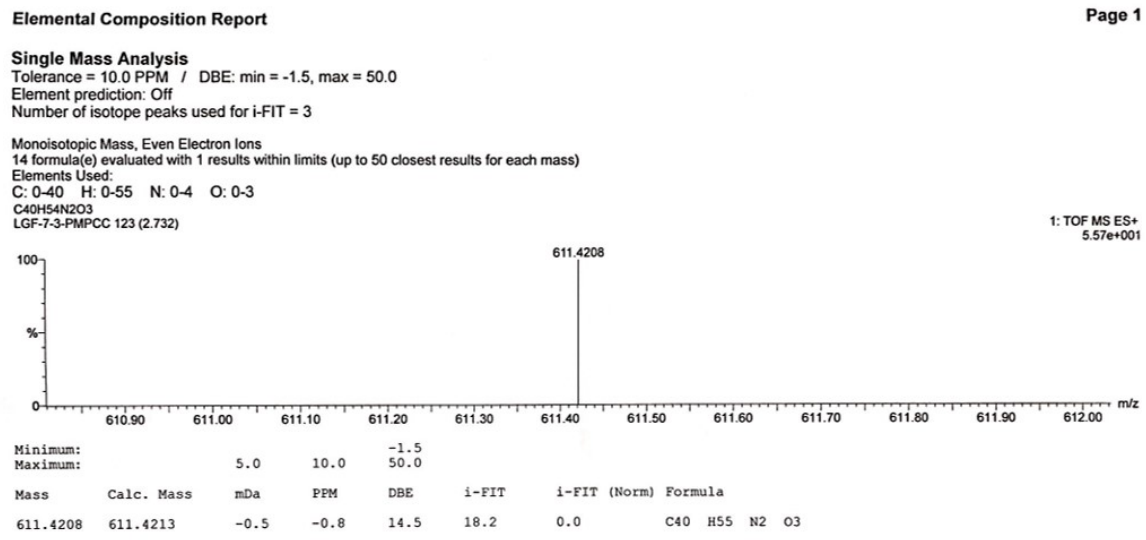

Figure S3. HR MS of mPMPCC.

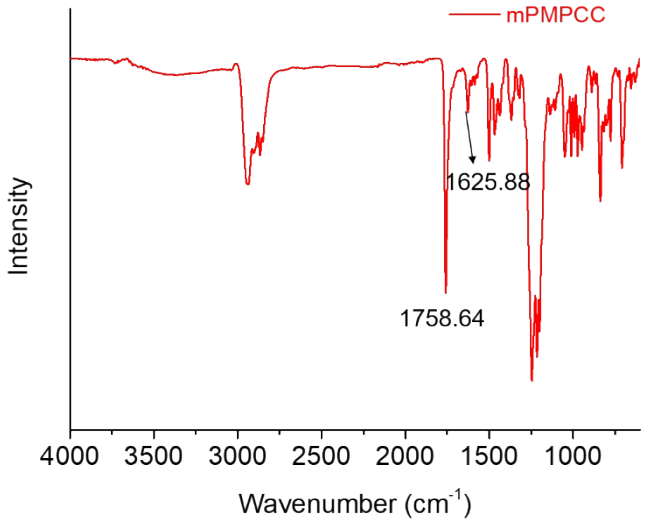

Figure S4. FT-IR spectra of mPMPCC powder. The 1758.64 cm^{-1} and 1625.88 cm^{-1} are assigned to the characteristic peaks of carbonyl bond in carbonate and imine bond, respectively.[1, 2]

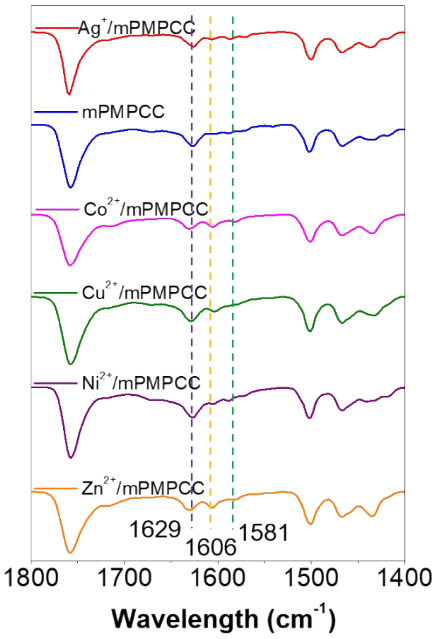

Figure S5. FT-IR spectra of mPMPCC powder and the complexes of Ag^{+}/mPMPCC, Co^{2+}/mPMPCC, Cu^{2+}/mPMPCC, Ni^{2+}/mPMPCC, and Zn^{2+}/mPMPCC. The bands of ~1581 cm^{-1} and ~1629 cm^{-1} are assigned to the characteristic peaks of pyridyl moiety and imine bond, respectively, while the newly band is observed around 1606 cm^{-1}, confirming a strong coordination of the nitrogen atom from the aromatic ring (pyridyl) with the metal ions.[2-4]

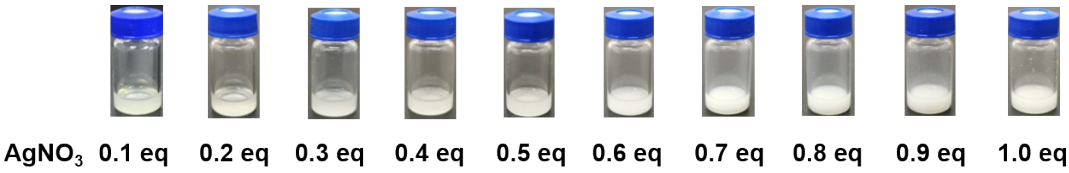

Figure S6. Photo images of mPMPCC+$AgNO_3$ based aggregates with adding various equivalent of Ag^+ in p-xylene/i-PrOH (v/v, 5 5). The concentration of mPMPCC was fixed at 16 mM.

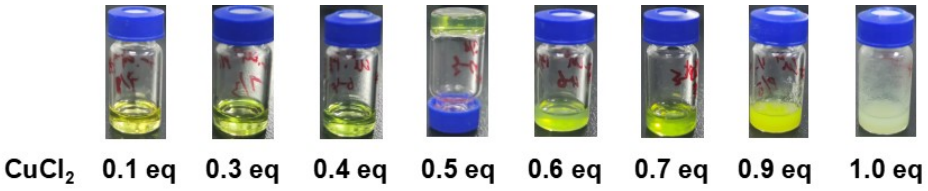

Figure S7. Photo images of mPMPCC+$CuCl_2$ mixtures by adding various equivalent of Cu^{2+} in p-xylene/i-PrOH (v/v, 5 5). The concentration of mPMPCC was fixed at 16 mM.

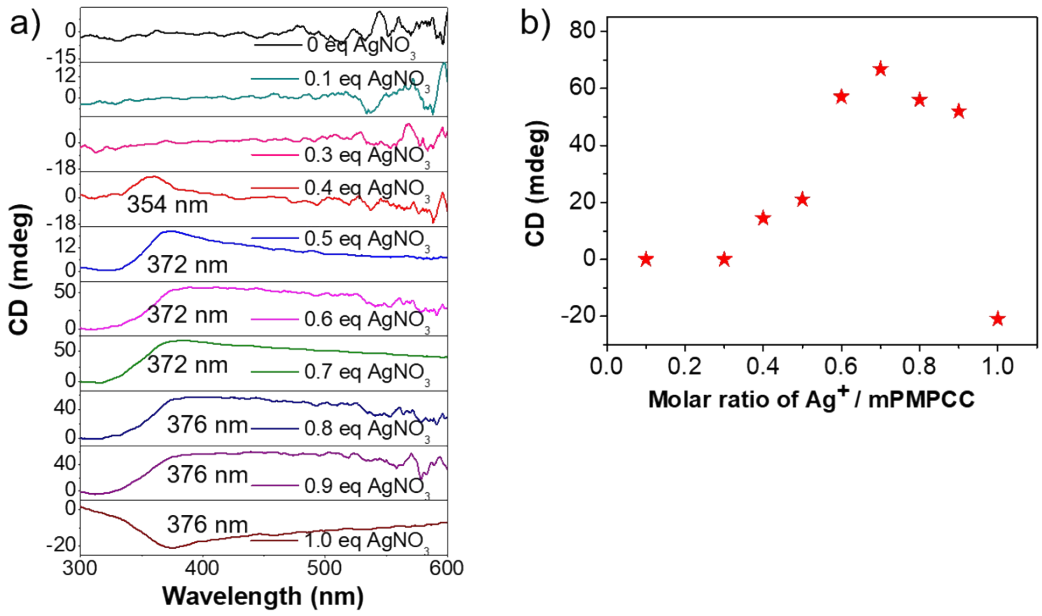

Figure S8. a) CD spectra of mPMPCC+$AgNO_3$ based aggregates with adding various equivalents of Ag^+ in p-xylene/i-PrOH (v/v, 5 5). b) the CD intensity of Ag^+ based aggregates as a function of molar ratios of $CuCl_2$ to mPMPCC. The concentration of mPMPCC was fixed at 16 mM.

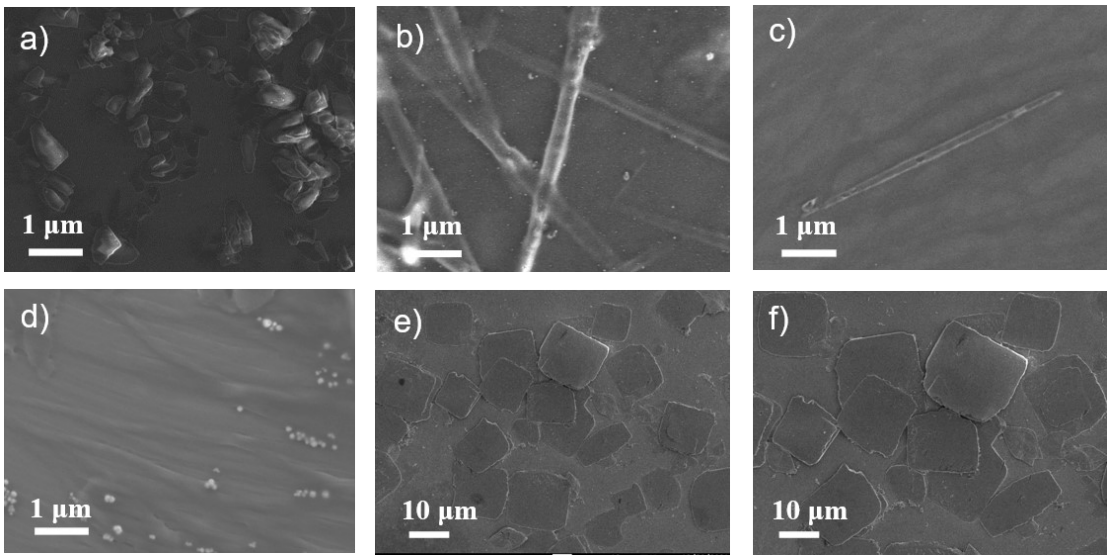

Figure S9. SEM images of mPMPCC with $AgNO_3$ in a) i-PrOH, b,c) p-xylene/i-PrOH (v/v, 3 7), d) p-xylene/i-PrOH (v/v, 5 5) and e,f) p-xylene/DMSO (v/v, 100 1). The concentration of mPMPCC was at 16 mM and the molar ratio of mPMPCC to metal ions was fixed at 2 1.

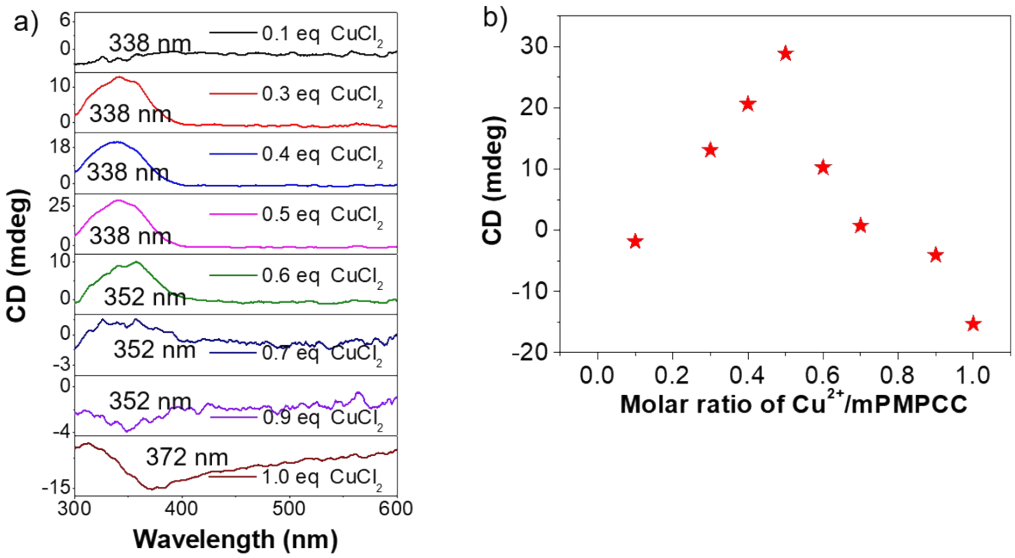

Figure S10. a) CD spectra of mPMPCC+$CuCl_2$ based aggregates with adding various equivalents of Cu^{2+} in p-xylene/i-PrOH (v/v, 5 5); b) the CD intensity of Cu^{2+} based aggregates as a function of molar ratios of $CuCl_2$ to mPMPCC. The concentration of mPMPCC was fixed at 16 mM.

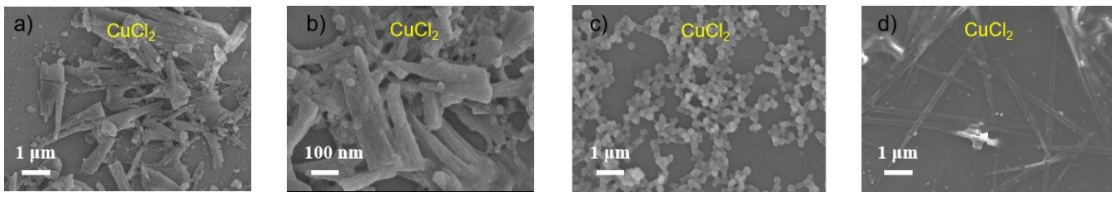

Figure S11. SEM images of mPMPCC+$CuCl_2$ based aggregates obtained from a,b) i-PrOH, c) p-xylene/n-butanol (v/v, 1 1) and d) p-xylene/i-PrOH (v/v, 5 5). The concentration of mPMPCC was 16 mM and the molar ratio of mPMPCC to Cu^{2+} was fixed at 2 1.

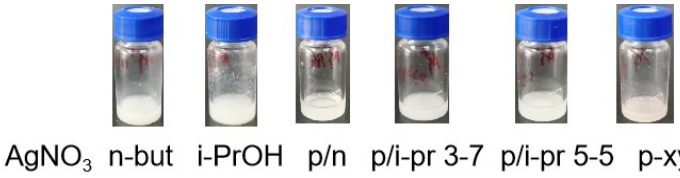

Figure S12. Photo images of mPMPCC (with the concentration of 16 mM) based metallogels formed by adding various solvents in Ag^{+}. The molar ratio of mPMPCC to metal ion was fixed at 2 1.

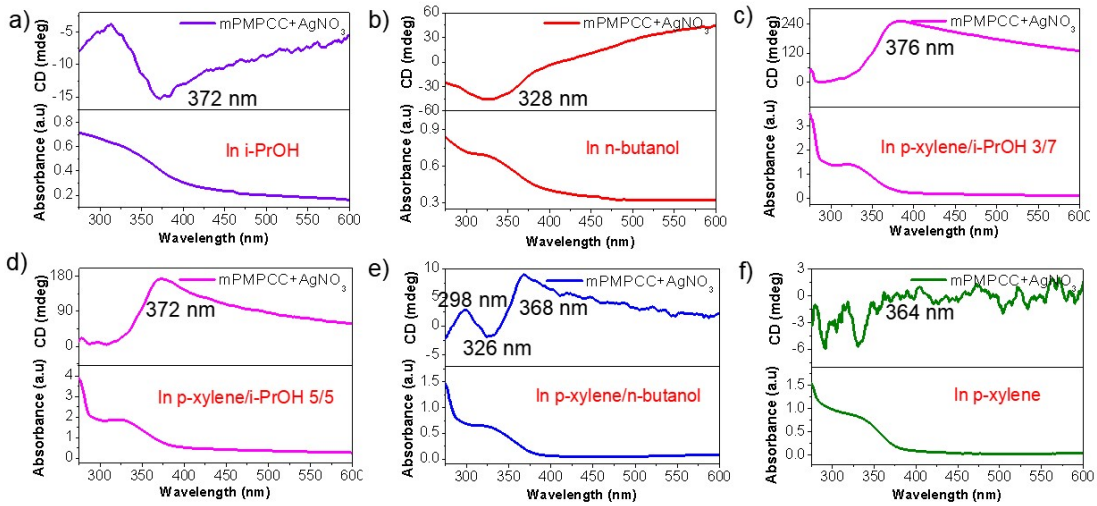

Figure S13. CD and corresponding UV-Vis spectra of mPMPCC+Ag^{+} based aggregates (with the concentration of mPMPCC at 16 mM) in a) i-PrOH, b) n-butanol, c) p-xylene/i-PrOH (v/v, 3 7), d) p-xylene/i-PrOH (v/v, 5 5), e) p-xylene/n-butanol (v/v, 1 1) and f) p-xylene/DMSO (v/v, 100 1).

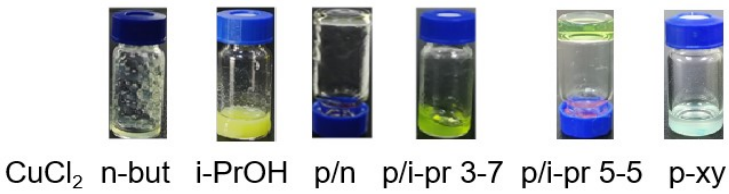

Figure S14. Photographs of mPMPCC+Cu^{2+} based aggregates in various solvents (with the concentration of mPMPCC at 16 mM and the molar ratio of mPMPCC to Cu^{2+} fixed at 2 1.

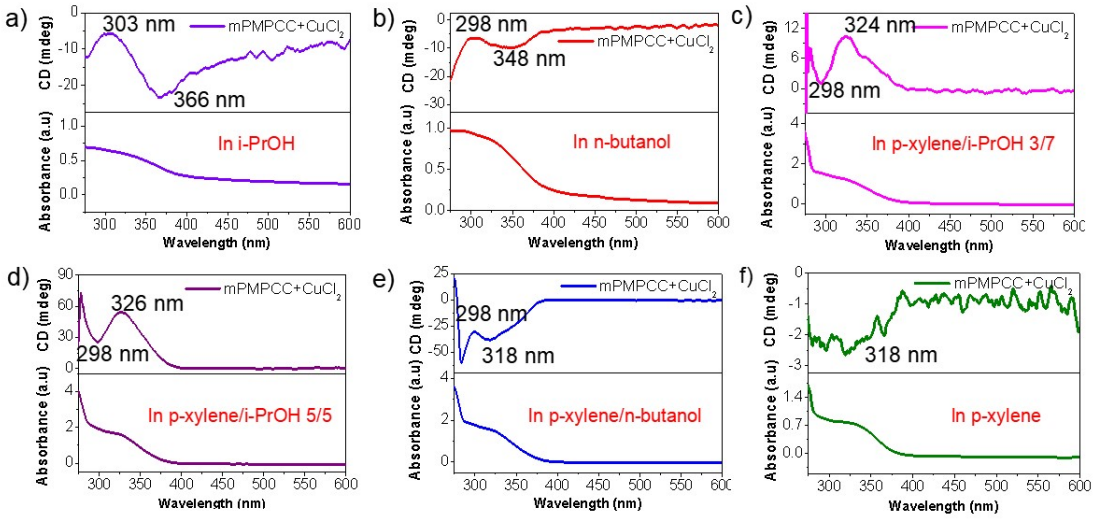

Figure S15. CD and corresponding UV-Vis spectra of mPMPCC+Cu^{2+} based aggregates (with the concentration of mPMPCC at 16 mM) in a) i-PrOH, b) n-butanol, c) p-xylene/i-PrOH (v/v, 3 7), d) p-xylene/i-PrOH (v/v, 5 5), e) p-xylene/n-butanol (v/v, 1 1) and f) p-xylene/DMSO (v/v, 100 1).

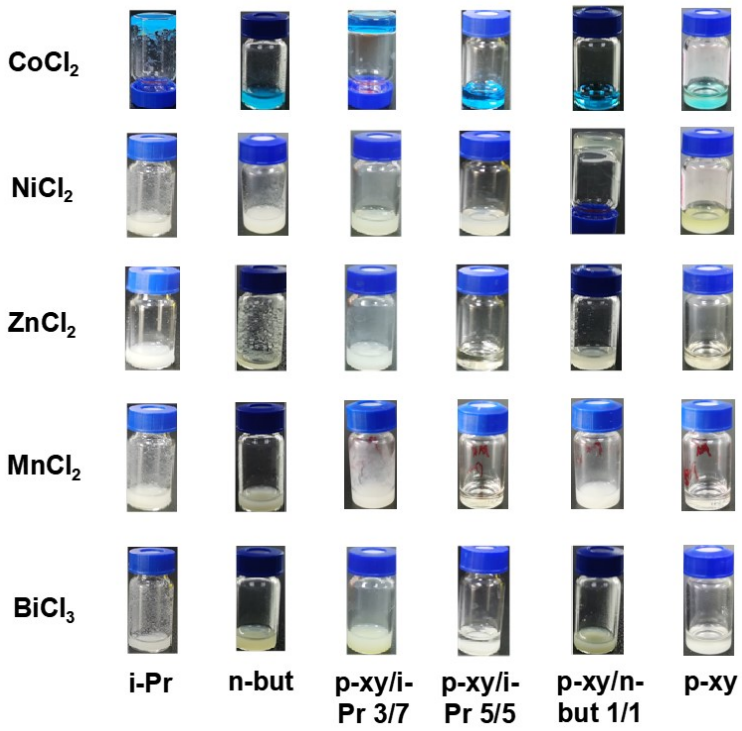

Figure S16. Photo images of aggregates of mPMPCC and various metal ions (including Co^{2+}, Ni^{2+}, Zn^{2+}, Mn^{2+}, and Bi^{3+}) in various solvents. The concentration of mPMPCC fixed at 16 mM and the molar ratio of mPMPCC to metal ion was fixed at 2 1.

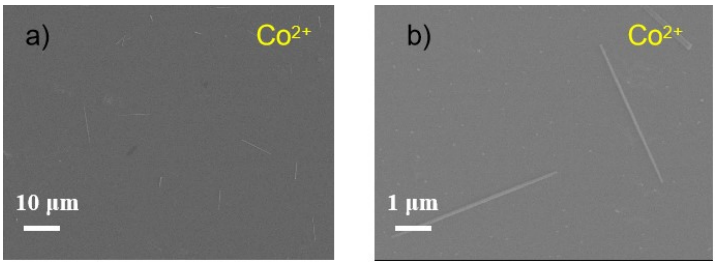

Figure S17. SEM images of mPMPCC+$CoCl_2$ aggregates (with the concentration of mPMPCC at 16 mM and the molar ratio of mPMPCC to Co^{2+} fixed at 2 1) in p-xylene/i-PrOH (v/v, 3 7).

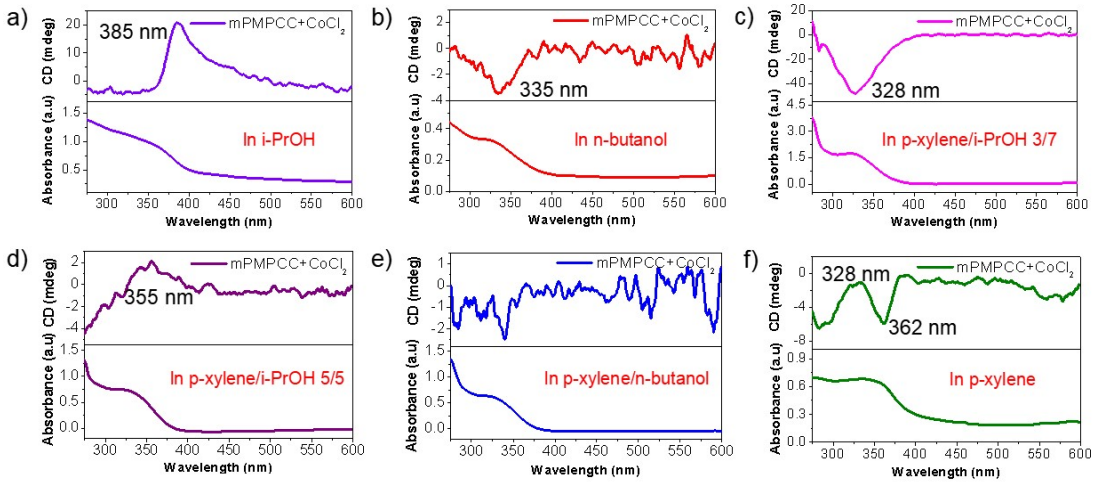

Figure S18. CD and corresponding UV-Vis spectra of mPMPCC+$CoCl_2$ (with the concentration of mPMPCC at 16 mM and the molar ratio of mPMPCC to Co^{2+} fixed at 2 1) in a) i-PrOH, b) n-butanol, c) p-xylene/i-PrOH (v/v, 3 7), d) p-xylene/i-PrOH (v/v, 5 5), e) p-xylene/n-butanol (v/v, 1 1) and f) p-xylene/DMSO (v/v, 100 1).

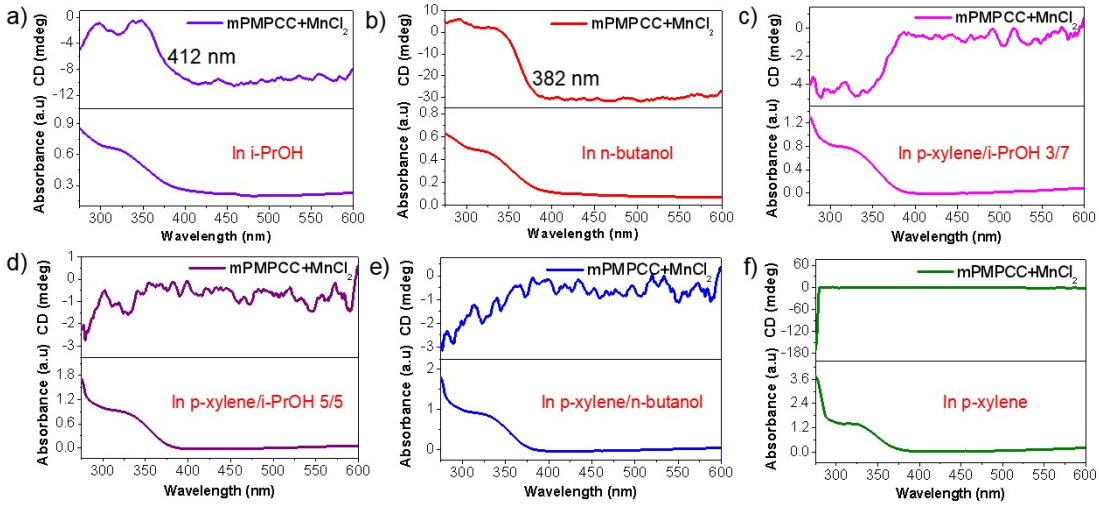

Figure S19. CD and corresponding UV-Vis spectra of mPMPCC+$MnCl_2$ (with the concentration of mPMPCC at 16 mM and the molar ratio of mPMPCC to Mn^{2+} fixed at 2 1) in a) i-PrOH, b) n-butanol, c) p-xylene/i-PrOH (v/v, 3 7), d) p-xylene/i-PrOH (v/v, 5 5), e) p-xylene/n-butanol (v/v, 1 1) and f) p-xylene/DMSO (v/v, 100 1).

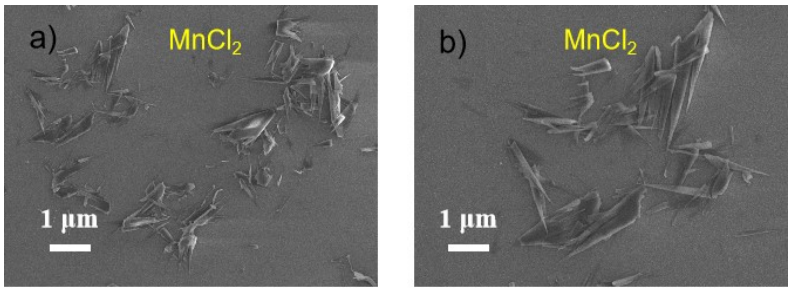

Figure S20. SEM images of mPMPCC+$MnCl_2$ aggregates in n-butanol (with the concentration of mPMPCC at 16 mM and the molar ratio of mPMPCC to Mn^{2+} fixed at 2 1).

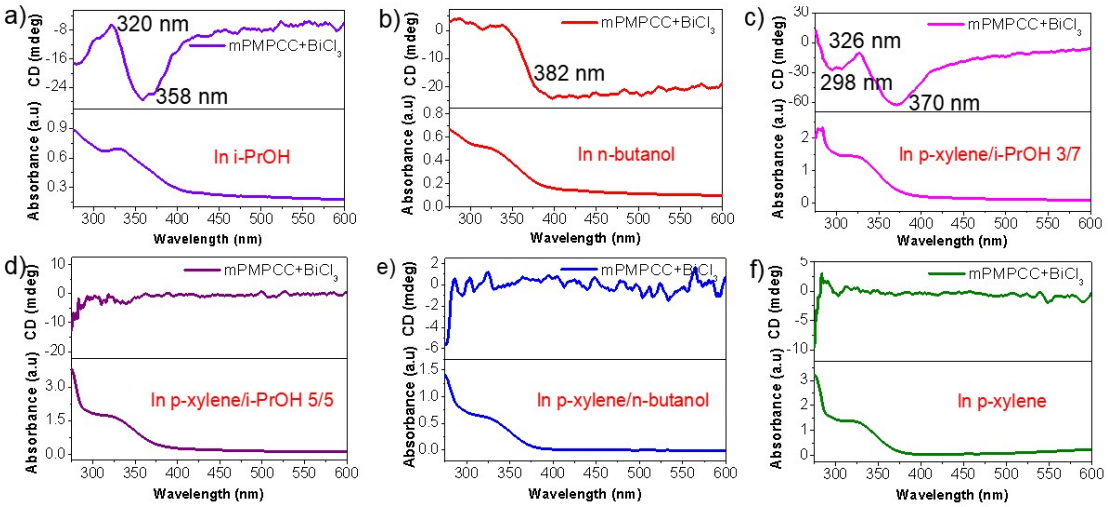

Figure S21. CD and corresponding UV-Vis spectra of mPMPCC+$BiCl_3$ (with the concentration of mPMPCC at 16 mM and the molar ratio of mPMPCC to Bi^{3+} fixed at 2 1) in a) i-PrOH, b) n-butanol, c) p-xylene/i-PrOH (v/v, 3 7), d) p-xylene/i-PrOH (v/v, 5 5), e) p-xylene/n-butanol (v/v, 1 1) and f) p-xylene/DMSO (v/v, 100 1).

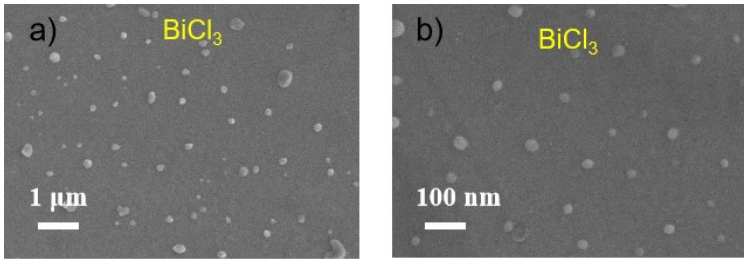

Figure S22. SEM images of mPMPCC+$BiCl_3$ aggregates in n-butanol (with the concentration of mPMPCC at 16 mM and the molar ratio of mPMPCC to Bi^{3+} fixed at 2 1).

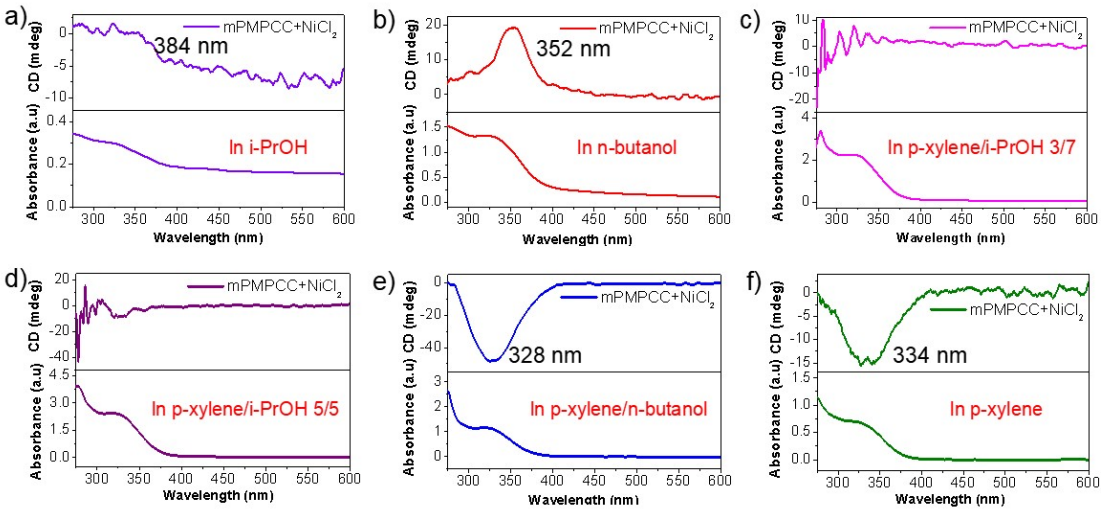

Figure S23. CD and corresponding UV-Vis spectra of mPMPCC+$NiCl_2$ (with the concentration of mPMPCC at 16 mM and the molar ratio of mPMPCC to Ni^{2+} fixed at 2 1) in a) i-PrOH, b) n-butanol, c) p-xylene/i-PrOH (v/v, 3 7), d) p-xylene/i-PrOH (v/v, 5 5), e) p-xylene/n-butanol (v/v, 1 1) and f) p-xylene/DMSO (v/v, 100 1).

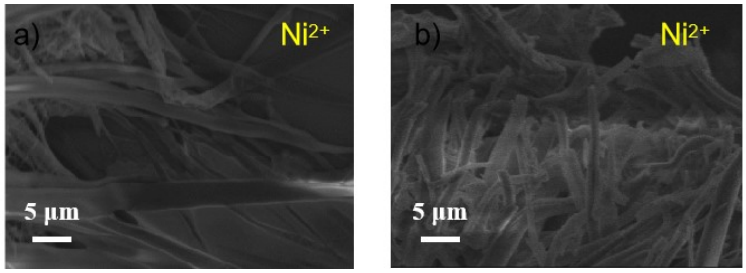

Figure S24. SEM images of mPMPCC+$NiCl_2$ aggregates in i-PrOH (with the concentration of mPMPCC at 16 mM and the molar ratio of mPMPCC to Ni^{2+} fixed at 2 1).

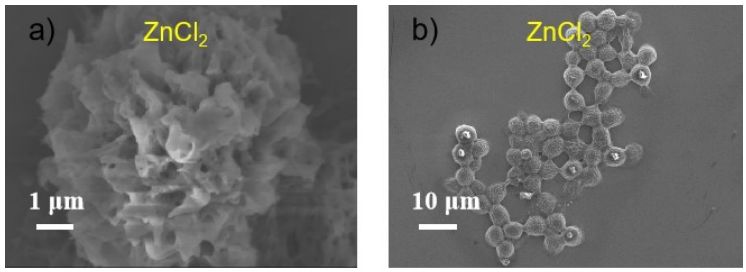

Figure S25. SEM images of mPMPCC+$ZnCl_2$ in a) i-PrOH and b) p-xylene/i-PrOH (v/v, 3 7). The concentration of mPMPCC was at 16 mM and the molar ratio of mPMPCC to Zn^{2+} was fixed at 2 1.

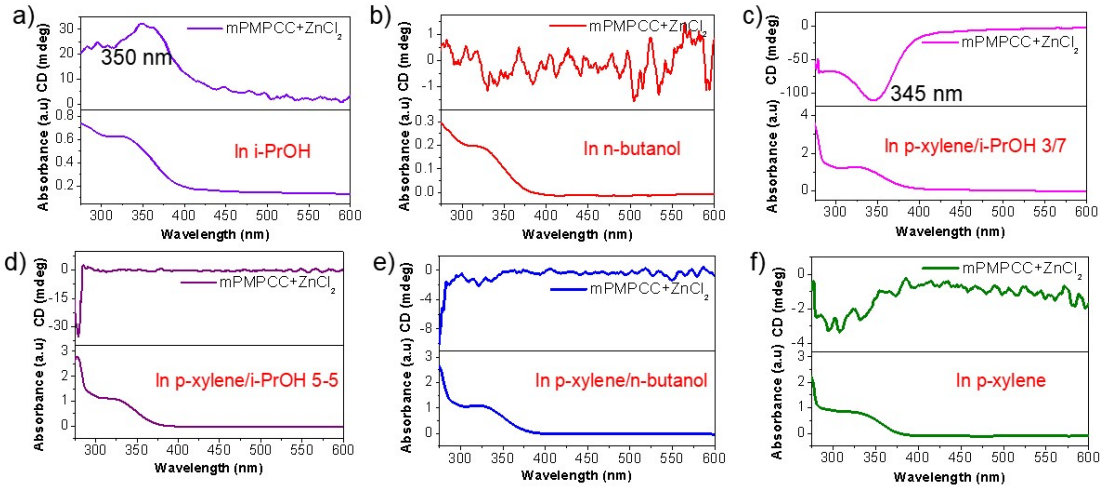

Figure S26. CD and corresponding UV-Vis spectra of mPMPCC+$ZnCl_2$ (with the concentration of mPMPCC at 16 mM and the molar ratio of mPMPCC to Zn^{2+} fixed at 2 1) in a) i-PrOH, b) n-butanol, c) p-xylene/i-PrOH (v/v, 3 7), d) p-xylene/i-PrOH (v/v, 5 5), e) p-xylene/n-butanol (v/v, 1 1) and f) p-xylene/DMSO (v/v, 100 1).

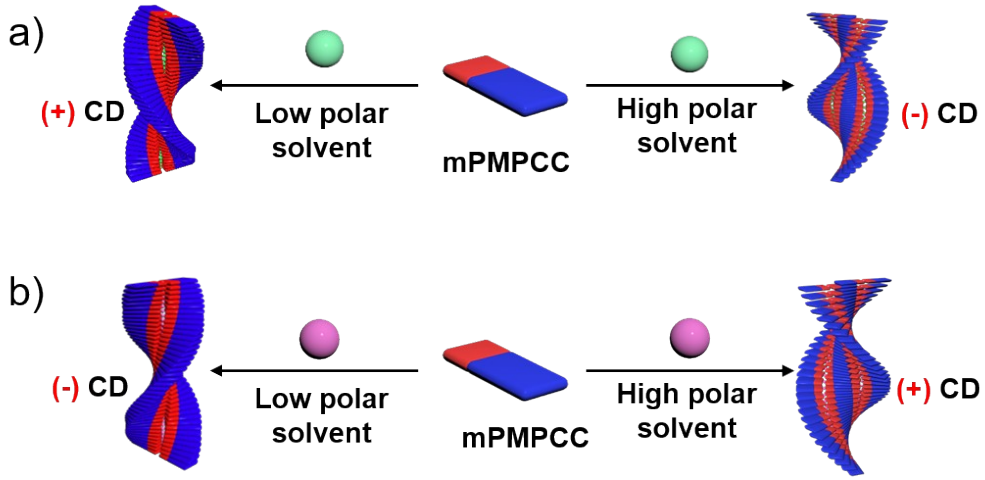

Figure S27. Proposed schematic illustration of supramolecular chirality inversion of metal-organic supramolecular polymers in CD spectra resulted from the solvents effect-induced molecular packing in a) Cu^{2+}, Ag^{+}, and b) Co^{2+}, Ni^{2+}, Zn^{2+}-based polymers system. The concentration of mPMPCC was at 16 mM and the molar ratio of mPMPCC to metal ions was fixed at 2 1.

a)

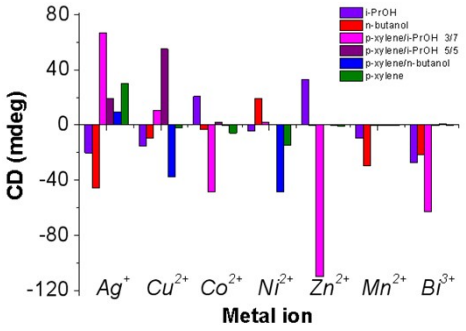

b)

	Ag^+	Mn^{2+}	Co^{2+}	Ni^{2+}	Cu^{2+}	Zn^{2+}	Bi^{3+}
n-butanol	−	−	−	+	−	N	−
i-PrOH	−	−	+	−	−	+	−
p-xylene/*n*-butanol (v/v, 5:5)	+	N	N	−	−	N	N
p-xylene/*i*-PrOH (v/v, 3:7)	+	N	−	+	+	−	−
p-xylene/*i*-PrOH (v/v, 5:5)	+	N	+	N	+	N	N
p-xylene	+	N	−	−	N	N	N

Figure S28. a) Proposed relationship between the CD absorption and corresponding chirality. b) Supramolecular chirality of nanostructures based on mPMPCC and metal ions regulated by metal ion and solvent effects. "+" represents positive Cotton effect, "–" represents negative Cotton effect, and "N" stands for negligible supramolecular chirality.

1. Liu, G.; Fu, K.; Wang, X.; Qian, C.; Liu, J.; Wang, D.; Wang, H.; Zhu, L.; Zhao, Y., One-Dimensional Helical Aggregates Organized from Achiral Imine-Based Polymers. *ACS Materials Letters* **2022,** *4* (4), 715-723.

2. Liu, G.; Sheng, J.; Teo, W. L.; Yang, G.; Wu, H.; Li, Y.; Zhao, Y., Control on Dimensions and Supramolecular Chirality of Self-Assemblies through Light and Metal Ions. *Journal of the American Chemical Society* **2018,** *140* (47), 16275-16283.

3. Kurzajewska, M.; Kwiatek, D.; Kubicki, M.; Brzezinski, B.; Hnatejko, Z., New complexes of 2-(4-pyridyl)-1,3-benzothiazole with metal ions; synthesis, structural and spectral studies. *Polyhedron* **2018,** *148*, 1-8.

4. Marjani, K.; Mousavi, M.; Hughes, D. L., Synthesis and crystal structure determination of copper(II) and iron(III) complexes of 2-(2-pyridyl)benzothiazole. *Transition Metal Chemistry* **2008,** *34*, 85-89.